A General Concept for Solar Water-Splitting Monolithic Photoelectrochemical Cells Based on Earth-Abundant Materials and a Low-Cost Photovoltaic Panel

Sitthichok Kasemthaveechok, Kiseok Oh, Bruno Fabre, Jean-Francois Bergamini, Cristelle Mériadec, Soraya Ababou-Girard, Gabriel Loget

DOI: 10.1002/((please add manuscript number))
Article type: Communication

A general concept for solar water-splitting monolithic photoelectrochemical cells based on earth-abundant materials and a low-cost photovoltaic panel

*Sitthichok Kasemthaveechok, Kiseok Oh, Bruno Fabre, Jean-François Bergamini, Cristelle Mériadec, Soraya Ababou-Girard and Gabriel Loget**

S. Kasemthaveechok, K. Oh, Dr. B. Fabre, J.-F. Bergamini and Dr. Gabriel Loget
Univ Rennes, CNRS, ISCR (Institut des Sciences Chimiques de Rennes)-UMR6226, F-35000 Rennes, France.
E-mail: gabriel.loget@univ-rennes1.fr
Cristelle Mériadec, Dr. Soraya Ababou-Girard
Univ Rennes, CNRS, IPR (Institut de Physique de Rennes)-UMR6251, F-35000 Rennes, France.

Keywords: artificial photosynthesis, water splitting, silicon, nickel

Alike photosynthesis, where light is transformed into energy-rich molecules, sunlight energy can be converted into H_2 and O_2 using water-splitting photoelectrochemical cells (PECs). These systems are highly promising to produce H_2 without carbon emission, however, their fabrication is still based on expensive fabrication procedure and non-abundant materials, which prevents their manufacturing and study by many laboratories. Here, we demonstrate an original concept for preparing monolithic water-splitting PECs based on the integration of a low-cost Si photovoltaic (PV) panel with two Si-based photoelectrodes fabricated by simple procedures and earth-abundant materials. In contrast with previous approaches, in the present system, the PV solid junction and the two solid/liquid junctions participate in the creation of the effective photovoltage applied for water splitting. This simple device that can split water from various electrolytes for several hours should promote new advances in the field of solar fuels.

Although the integration of solar and wind energies in electrical grids is considerably growing worldwide, a major concern in employing these energy sources to a much larger extent is their

intermittency and their diffuse geographic distribution.[1] A solution to solve these two issues is the conversion of renewables into a carbon-free energy carrier that would allow the storage and distribution of energy on site and on demand.[2] Hydrogen (H_2) has long been considered an ideal energy carrier because it has a higher density per mass unit than gasoline and Li-ion batteries and can be readily used to provide energy to buildings and energy-intensive transportation systems. To this goal, H_2 must be generated through a zero-emission process. This is possible by coupling water electrolysis to a renewable source of energy to yield highly pure H_2 only from water. In the specific case of solar-to-H_2 energy conversion, two main strategies are currently investigated.[3,4] The first method consists in spatially decoupling light absorption with gas production by using assemblies of photovoltaic (PV) panels connected to metal electrodes.[5–8] The second approach is based on integrated systems, referred as monolithic photoelectrochemical cells (PECs), devices that are composed of semiconductor (SC) absorber surfaces which, alike photosynthesis, can convert the incident photons into a chemical fuel (*e.g.* H_2, MeOH, CO). Usually, the illuminated SC junction provides the potential required to trigger the overall reaction, which is applied to co-catalysts (*cocat*) layers, where the electrolysis takes place. Several examples of PECs triggering spontaneously water electrolysis under solar irradiation have been reported to date, the most efficient systems being based on III-V SCs coupled with expensive *cocats* such as Pt and IrO_2.[9–13] It is generally admitted that the practical use of PEC will be envisioned only when their cost will be reduced,[14] thus, intense research efforts are currently devoted to the manufacturing of PECs based on abundant absorbers and *cocat* materials. Silicon (Si) is one of the most attractive absorbers to be used for PECs because it has a band gap small enough for allowing an optimal absorption of the solar spectrum (1.1 eV), it is very abundant and widely used by the microelectronics and photovoltaic industries.[15] Nevertheless, using Si as a photoelectrode material is highly challenging because it is prone to rapid deactivation by spontaneous oxidation and chemical etching in aqueous electrolytes.[16] Recent reports have shown that Ni-

based catalysts, in the form of thin films or particles, deposited on Si photoelectrodes are excellent coating materials as they confer corrosion resistance and high catalytic activity for both water splitting half-reactions, namely, hydrogen evolution reaction (HER)[17–20] and oxygen evolution reaction (OER)[21–25] at high pH.

If a few examples of monolithic PEC devices based exclusively on Si absorbers and Ni *cocats* have been reported to date, they are all based on a rather similar design where a SC solid junction (*e.g. a*-Si triple junction) generates an important potential (> 2 V) that is applied to the *cocat* thin film or to metal electrodes for water splitting.[5,26,27] Herein, we demonstrate an original monolithic approach based on the integration of a low-cost (< 5 €) Si PV panel with two Si photoelectrodes fabricated by easy procedures and earth-abundant materials. Unlike the previous strategies, in the present system, the three illuminated elements (the PV solid junction and the two solid/liquid junctions) participate in the generation of the effective photovoltage applied for water splitting. We demonstrate that this simple device can produce H_2 with a high current and a quantitative faradaic efficiency for more than 7 hours.

We will first describe both photoelectrodes individually before combining them in a monolithic device. The photoanodes were prepared by electrodeposition of Ni^0 from an aqueous electrolyte on *n*-Si (100) wafers, which led to the uniform decoration of the Si surface with randomly-dispersed hemispherical Ni nanoparticles (NPs) (diameter = 48 ±19 nm, height = 30 ±10 nm) as shown by the atomic force microscopy (AFM) and scanning electron microscopy (SEM) images (**Figure 1c** and S1). After deposition, the modified Si surface was cut and an insulating resin was deposited to define an active surface area of 0.45 cm^2 (the value used for all electrodes in this study). Afterwards, the surface was conditioned by photoelectrochemical activation, which consisted in applying hundred cyclic voltammetry (CV) scans to the illuminated photoanode in a O_2-saturated 1 M NaOH solution in order to generate a high-activity $Ni(OH)_2$-NiOOH catalytic shell around the particles, known to

considerably improve the OER kinetics (Figure S2).[28] X-ray photoelectron spectroscopy (XPS), performed on an activated surface (referred as *n*-Si/Ni NPs_{act}) confirmed the presence of the expected elements: Ni, Si as well as O originating from the SiO_x layer and the Ni hydroxides generated during activation (Figures 1e, S3 and S4).[28] Figure 1a shows the CVs recorded with this surface (red and black curves) and compares them with benchmark anodes in Ar-saturated 1 M NaOH solution.

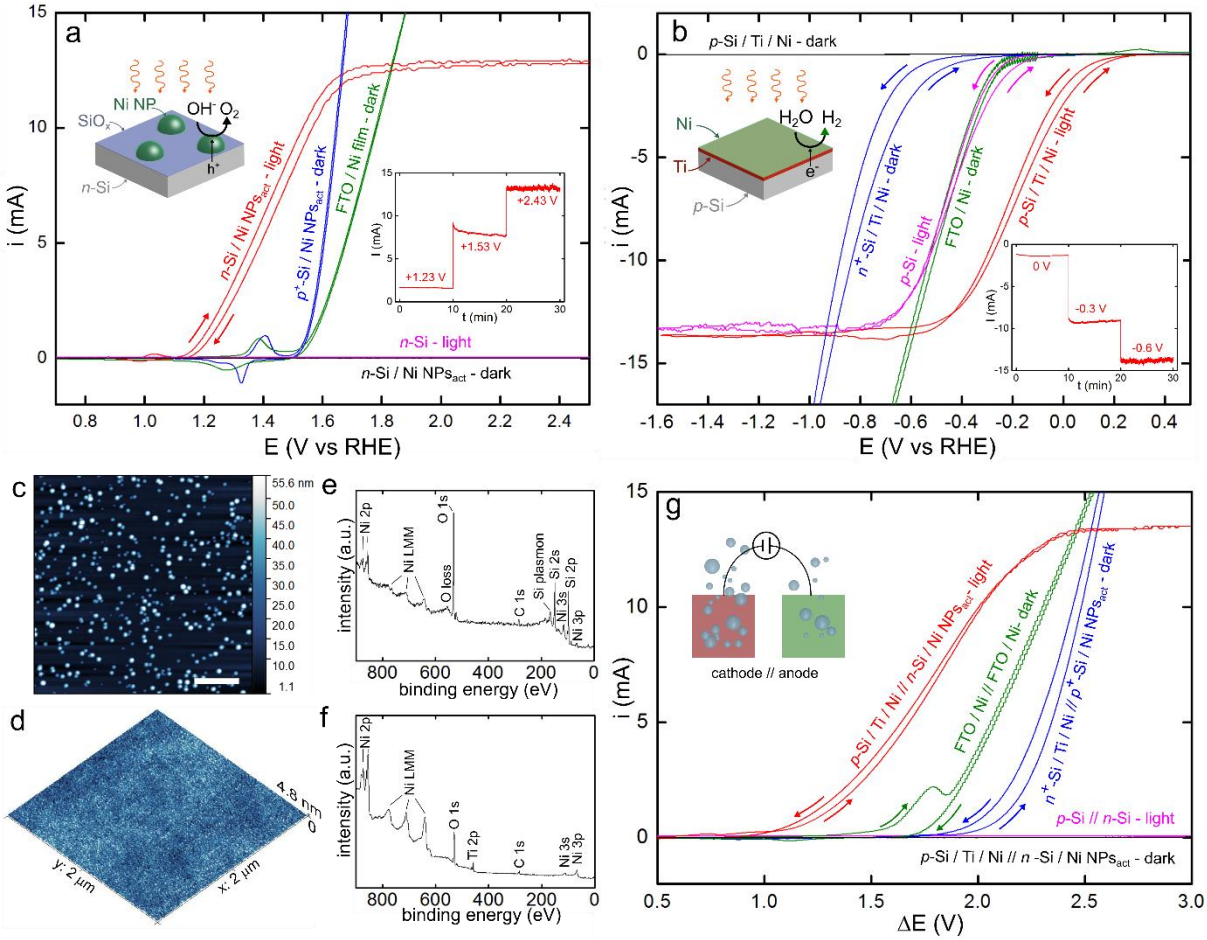

Figure 1. Characterization of the photoelectrodes. a,b) CVs recorded in Ar-saturated 1 M NaOH in the dark or under AM 1.5G illumination with: a) *n*-Si/Ni NPs_{act} in the dark (black) and under illumination (red), *n*-Si under illumination (pink), Ni NPs-modified p^+-Si after activation in the dark (blue), a FTO surface coated with a 50 nm-thick Ni thin film (green); and b) *p*-Si/Ti/Ni in the dark (black) and under illumination (red), *p*-Si under illumination (pink), n^+-Si/Ti/Ni in the dark (blue) and an FTO surface coated with a 1 nm-thick Ni thin film (green). Insets: schemes showing the photoelectrodes in operation (top left corners); series of CA measurements obtained for the best performing photoelectrodes (bottom right corners). c,d) AFM images of: c) Ni NPs-modified *n*-Si surface (the scale bar equals 1 µm) and d) the Ni/Ti coated *p*-Si surface. e,f) XPS survey spectra of the corresponding photoelectrodes. g) CVs recorded in a two electrodes configuration in 1 M NaOH in the dark

or under AM 1.5G illumination for the different sets of cathode // anode, as indicated in the figure. The sweep direction are indicated by arrows.

First, it can be observed that bare *n*-Si under illumination did not promote OER (pink curve). This was caused by Si self-oxidation that electrically passivated the surface with a SiO_x layer (Figure S5). In contrast, the presence of Ni NPs on the Si surface allowed to obtain a considerable OER catalytic current under illumination (red curve). This photoanode exhibited better performance than a 50 nm-thick sputtered Ni thin film (green curve) and activated Ni NPs on a non-photoactive p^+-Si surface (blue curve). The comparison between the red and the blue curves, allows estimating a photovoltage of 0.37 V (Figure S6). The chronoamperometry (CA) curves (inset of Figure 1a) shows that the catalytic currents were stable at different OER potentials.

The preparation of the photocathodes was inspired by the method from Dai et al.[17] We made them by successively depositing a 5 nm-thick Ti and a 1 nm-thick Ni coatings on a freshly hydrogenated *p*-Si (100) wafer by magnetron sputtering (the surface is referred as *p*-Si/Ti/Ni). The Ti film acted as a stabilizing layer, preventing the Si alkaline corrosion and, additionally, improved the photovoltage by generating a high Schottky barrier at the Si/Ti interface. The overlying Ni serves as a HER *cocat*.[17,29] The homogeneity of the coating was confirmed by AFM (Figure 1d, root-mean-square roughness = 0.5 nm). Energy dispersive X-ray spectroscopy (EDS, Figure S7) and XPS (Figures 1f, S3 and S4) confirmed the presence of the expected elements (Ni, Ti, and O), note that here the O signal originates mainly from the Ti and Ni surface oxides. Figure 1b shows the CVs obtained with these surfaces and benchmark cathodes in Ar-saturated 1 M NaOH. The best performance was obtained with the illuminated *p*-Si/Ti/Ni (red curve) that triggered HER at an onset potential of about +0.2 V vs Reversible Hydrogen Electrode (RHE). In contrast, at an illuminated hydrogenated *p*-Si, the reaction started at an onset potential negatively shifted by at least 0.2 V (pink curve) and very similar to that of a 1 nm-thick Ni film on fluorine-doped tin oxide (FTO) (green curve). The

worst HER characteristics were obtained with the non-photoactive n^+-Si surface modified in the same way as the *p*-Si/Ti/Ni, which exhibited an onset potential more than 0.55 V negative from *p*-Si/Ti/Ni (Figure S6). This surprisingly negative onset potential suggests that the n^+-Si/Ti interface degrades the Ni HER performance and highlights the importance of the doping of the Si substrate for the Ti/Ni system to operate efficiently. The good stability of the illuminated *p*-Si/Ti/Ni was further confirmed by the CA curves shown in the inset of Figure 1b.

We now combine the pairs of electrodes (denoted here cathode // anode) whose performance was individually described and we study their behavior when connected in a two-electrode fashion, as shown in Figure 1g. One can observe that uncoated and freshly hydrogenated *p*-Si // *n*-Si under illumination (pink curve) did not produce noticeable photocurrent due to the *n*-Si passivation (*vide supra*). Logically, *p*-Si/Ti/Ni // *n*-Si/Ni NPs_{act} in the dark did not trigger water splitting due to the lack of minority charge carriers at each electrode. In contrast, all other systems allowed to electrolyze water with onset potentials consistent with those being determined previously for each half-reaction separately (Figure 1a,b). It is interesting to note that the Ni thin films deposited on FTO (FTO/Ni // FTO/Ni, green curve) exhibited better performance than the non-photoactive Si-supported system (n^+-Si/Ti/Ni //p^+-Si/Ni NPs_{act}, blue curve), due to the low performance of the n^+-Si/Ti/Ni cathode (Figure 1b). The best performance within the low potential range (from +1 to +2 V) was by far obtained with the illuminated *p*-Si/Ti/Ni // *n*-Si/Ni NPs_{act} system, which triggered water splitting starting from about +1 V and reached a light-limited photocurrent of 13.4 mA, in good agreement with the results obtained for the photoanode and photocathode, individually (red curves in Figure 1a,b). This value of onset potential is much smaller than that obtained with all the other systems (blue and green curves) and demonstrates the beneficial effect of the cumulated photovoltage generated at both solid/liquid interfaces.

As commercially available miniaturized Si PV panels are able to generate a potential in this range, we interfaced this pair of photoelectrodes with a low-cost PV panel, as we will describe in the following.

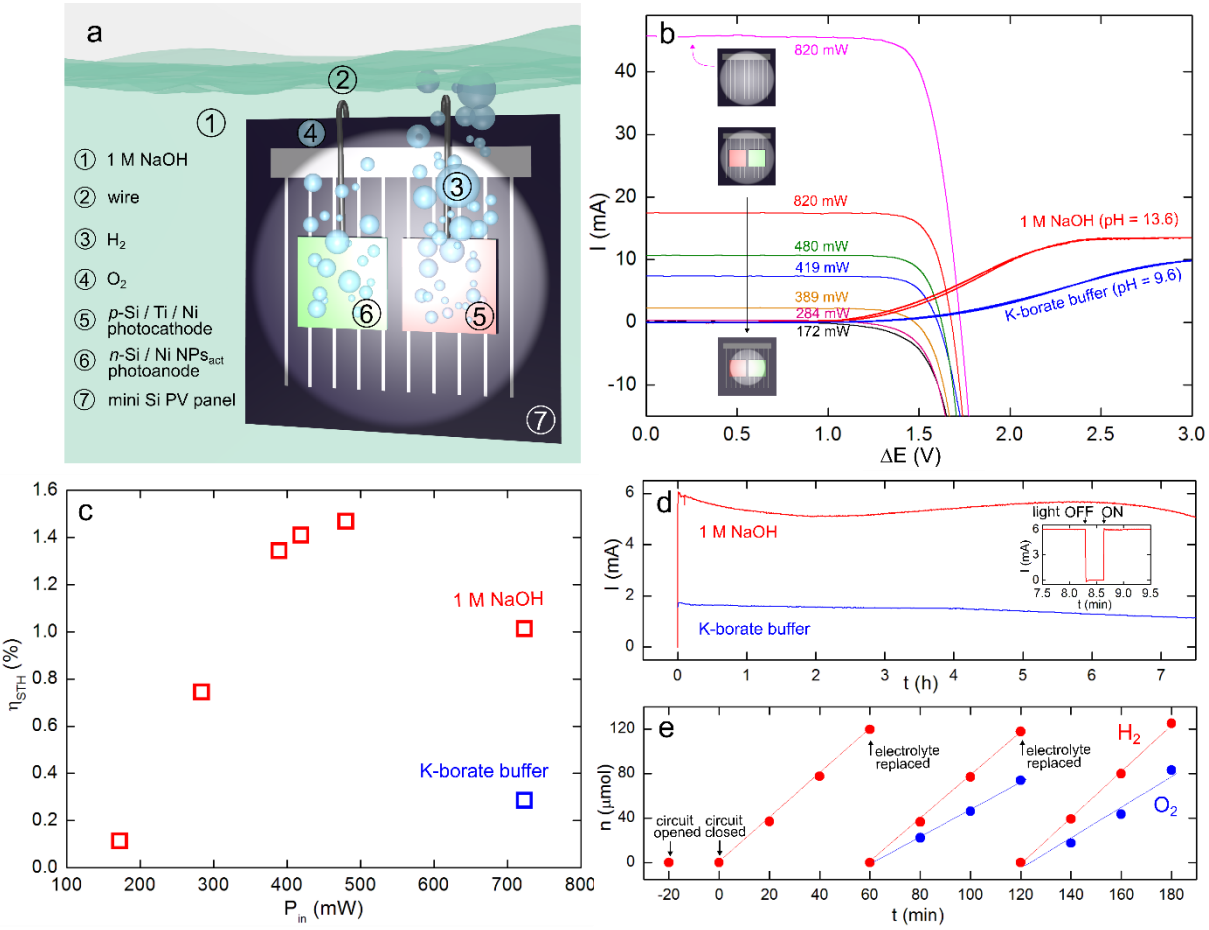

Fig. 2. Water photosplitting cell. a) Scheme showing the elements of the PEC device in operation in 1 M NaOH. b) *I* - *E* curves obtained for the PV panel immersed in 1 M NaOH and illuminated with AM 1.5G (thin lines) in the following modes: without photoelectrodes (pink), with the pair of photoelectrodes immobilized on the surface (red), and by decreasing the diameter of the incident light spot (green to black), the input power is indicated for each curve. Thick lines are CVs recorded in a two electrodes configuration under AM 1.5G illumination for *p*-Si/Ti/Ni // *n*-Si/Ni NPs_{act} in NaOH (red) and K-borate buffer (blue). c) Plot of the solar-to-H_2 efficiency as a function of the input power, in NaOH (red) and in K-borate buffer (blue). d) Current flowing through the illuminated PEC (P_{in} ~820 mW) during preparative-scale water-splitting experiments in NaOH (red) and K-borate buffer (blue). Inset: curve showing the current evolution in NaOH when illumination is interrupted. e) Plots showing the number of moles of H_2 (red) and O_2 (blue) evolved in NaOH as a function of the time, disks are experimental points, lines are linear fits.

Figure 2a depicts the PEC system (digital photographs are shown in Figure S8b), with the two photoelectrodes immobilized on the front side of the 4×4 cm² PV panel using an inert

epoxy resin and the PV wires connected to the photoelectrodes. The PEC assembly was placed in a single-compartment home-made glass cell (Figure S9a) that contained the electrolyte, a construct that is beneficial in terms of space optimization and can be used with a solar simulator having a rather small beam diameter (3.5 cm in our case). Solar water splitting was directly evidenced by the appearance of bubbles at both electrodes under illumination with simulated sunlight (video in SI). When needed, the current flowing through the system could be measured by connecting the PEC device to a potentiostat that did not apply bias (acting as an ammeter). In our design, the photoelectrodes masked a part of the active surface PV panel, which affected its *I-E* characteristics (pink *vs* red curve in Figure 2b), however, this was not detrimental as the PV panel can generate much more current than what the photoelectrodes can afford, according to these curves, the shadowing would lead to an overall current decrease of ~ 1mA. That being said, it becomes obvious that the spot size has a crucial importance for the device performance. Assuming a faradaic efficiency (η_F) of 100 % (*vide infra*), the solar-to-H_2 efficiency (η_{STH}) can be calculated according to the following equation:[4]

$$\eta_{\mathrm{STH}}(\%) = \frac{I\,(\mathrm{mA}) \times 1.23\,(\mathrm{V})}{P_{\mathrm{in}}\,(m\mathrm{W})} \times 100 \qquad (1)$$

where I is the current flowing through the device, 1.23 V is the thermodynamic potential of water electrolysis and P_{in} is the power of the incident light beam. We have studied η_{STH} as a function of the spot size, that is, as a function of P_{in}. The results, shown in Figure 2c, were obtained by using equation (1) with I being the average current flowing through the PEC device during 15 min of electrolysis (Figure S10, Table S1). Remarkably, η_{STH} followed a parabolic trend with a maximum experimental value of 1.5 % at P_{in} ~ 480 mW, which corresponds to a spot diameter of ~2.5 cm. Additionally, the system was tested in another electrolyte with a reduced pH (2 M potassium borate, pH = 9.6). If water splitting worked

under these conditions, this electrolyte yielded considerably smaller η_{STH} as a result of the lower water electrolysis kinetics (blue CV in Figure 2b).

The stability of the device was tested during preparative-scale electrolysis under illumination. As it can be seen in the red curve of Figure 2d, the system could electrolyze water for 7.5 h in 1 M NaOH, which is remarkable in such a Si-corrosive solution. As expected, interruption of illumination stopped water electrolysis, as demonstrated by the instantaneous decrease of the catalytic current to zero (inset of Figure 2d). In addition, gas analysis was performed to determine the reaction products in the headspace (Figure 2e).When the electrical circuit was opened, neither H_2 nor O_2 were detected, confirming that the gas evolution was not a result of a spontaneous chemical reaction or a degradation product. As soon as the circuit was closed, the gas evolution took place, with an H_2 to O_2 molar ratio of 1.6, close to the expected stoichiometry of 2. To test the reproducibility of our system, several successive runs were performed with a fresh electrolyte (Figure 2e and S11). Based on the recorded CA curves and the amount of produced H_2, we calculated for each run a η_F comprised between 96 and 102%, demonstrating a quantitative water electrolysis and confirming the exactness of equation (1). At a lower pH (blue curve) the PEC still delivered a significant current after 13 h of electrolysis (Figure S12). The PV panel showed an excellent resistance under the electrolysis conditions and could be re-employed many times to manufacture many PECs.

In conclusion, we have reported a new concept for the fabrication of water splitting monolithic PECs, based on abundant materials, simple processes and low-cost commercial PV panels. This system produces H_2 with a quantitative faradaic efficiency and operates for several hours before showing signs of degradation, in a very corrosive medium for the Si material (1 M NaOH). We have shown that the solar-to-hydrogen efficiency depends on the size of the illuminated area and design optimization should lead to significant improvement in

the near future. Progress is now underway to separate the gas products. Such a simple design should considerably democratize the use of monolithic PECs in many laboratories and should lead to considerable improvements in the field of solar fuels.

Supporting Information
Supporting Information is available from the Wiley Online Library or from the author.

Acknowledgements
This work is partly funded by ANR (project EASi-NANO, ANR-16-CE09-0001-01). Cécile Valter-Potier is acknowledged for fabrication of the photoelectrochemical cells. Francis Gouttefangeas and Loic Joanny (ScanMAT-CMEBA, Univ. Rennes 1) are fully acknowledged for SEM imaging.

Received: ((will be filled in by the editorial staff))
Revised: ((will be filled in by the editorial staff))
Published online: ((will be filled in by the editorial staff))

References

[1] N. S. Lewis, D. G. Nocera, *Proc. Natl. Acad. Sci.* **2006**, *103*, 15729–15735.

[2] D. Elliott, *Nat. Energy* **2016**, 15003.

[3] A. Rothschild, H. Dotan, *ACS Energy Lett.* **2017**, *2*, 45–51.

[4] J. W. Ager, M. R. Shaner, K. A. Walczak, I. D. Sharp, S. Ardo, *Energy Environ. Sci.* **2015**, *8*, 2811–2824.

[5] C. R. Cox, J. Z. Lee, D. G. Nocera, T. Buonassisi, *Proc. Natl. Acad. Sci. U. S. A.* **2014**, *111*, 14057–14061.

[6] M. A. Modestino, K. A. Walczak, A. Berger, C. M. Evans, S. Haussener, C. Koval, J. S. Newman, J. W. Ager, R. A. Segalman, *Energy Environ. Sci.* **2014**, *7*, 297–301.

[7] T. J. Jacobsson, V. Fjallstrom, M. Sahlberg, M. Edoff, T. Edvinsson, *Energy Environ. Sci.* **2013**, *6*, 3676–3683.

[8] J. Luo, J.-H. Im, M. T. Mayer, M. Schreier, M. K. Nazeeruddin, N.-G. Park, S. D. Tilley, H. J. Fan, M. Grätzel, *Science* **2014**, *345*, 1593–1596.

[9] O. Khaselev, J. A. Turner, *Science* **1998**, *280*, 425–427.

[10] K. Sivula, R. van de Krol, *Nat. Rev. Mater.* **2016**, *1*, 15010.

[11] M. S. Prévot, K. Sivula, *J. Phys. Chem. C* **2013**, *117*, 17879–17893.

[12] M. G. Walter, E. L. Warren, J. R. McKone, S. W. Boettcher, Q. Mi, E. A. Santori, N. S. Lewis, *Chem. Rev.* **2010**, *110*, 6446–6473.

[13] S. Licht, B. Wang, S. Mukerji, T. Soga, M. Umeno, H. Tributsch, *J. Phys. Chem. B* **2000**, *104*, 8920–8924.

[14] M. R. Shaner, H. A. Atwater, S. Lewis, E. W. Mcfarland, *Energy Environ. Sci.* **2016**, *9*, 2354–2371.

[15] K. Sun, S. Shen, Y. Liang, P. E. Burrows, S. S. Mao, D. Wang, *Chem. Rev.* **2014**, *114*, 8662–8719.

[16] X. G. Zhang, *Electrochemistry of Silicon and Its Oxide*, Kluwer Academic, **2001**.

[17] J. Feng, M. Gong, M. J. Kenney, J. Z. Wu, B. Zhang, Y. Li, H. Dai, *Nano Res.* **2015**, *8*, 1577–1583.

[18] J. R. McKone, E. L. Warren, M. J. Bierman, S. W. Boettcher, B. S. Brunschwig, N. S. Lewis, H. B. Gray, *Energy Environ. Sci.* **2011**, *4*, 3573–3583.

[19] I. A. Digdaya, P. P. Rodriguez, M. Ma, G. W. P. Adhyaksa, E. C. Garnett, A. H. M. Smets, W. A. Smith, *J. Mater. Chem. A* **2016**, *4*, 6842–6852.

[20] J. Zhao, L. Cai, H. Li, X. Shi, X. Zheng, *ACS Energy Lett.* **2017**, *2*, 1939–1946.

[21] M. J. Kenney, M. Gong, Y. Li, J. Z. Wu, J. Feng, M. Lanza, H. Dai, *Science* **2013**, *342*, 836–840.

[22] S. Hu, M. R. Shaner, J. A. Beardslee, M. Lichterman, B. S. Brunschwig, N. S. Lewis, *Science* **2014**, *344*, 1005–1009.

[23] K. Sun, F. H. Saadi, M. F. Lichterman, W. G. Hale, H.-P. Wang, X. Zhou, N. T. Plymale, S. T. Omelchenko, J.-H. He, K. M. Papadantonakis, et al., *Proc. Natl. Acad. Sci. USA* **2015**, *112*, 3612–3617.

[24] G. Loget, B. Fabre, S. Fryars, C. Mériadec, S. Ababou-Girard, *ACS Energy Lett.* **2017**, *2*, 569–573.

[25] G. Xu, Z. Xu, Z. Shi, L. Pei, S. Yan, Z. Gu, Z. Zou, *ChemSusChem* **2017**, *10*, 2897 – 2903.

[26] R. E. Rocheleau, E. L. Miller, A. Misra, *Energy & Fuels* **1998**, *12*, 3–10.

[27] S. Y. Reece, J. A. Hamel, K. Sung, T. D. Jarvi, A. J. Esswein, J. J. H. Pijpers, D. G. Nocera, *Science* **2011**, *334*, 645–648.

[28] K. Oh, C. Meriadec, B. Lassalle-Kaiser, V. Dorcet, B. Fabre, S. Ababou-Girard, L. Joanny, F. Gouttefangeas, G. Loget, *submitted* **2018**.

[29] B. Seger, A. B. Laursen, P. C. K. Vesborg, T. Pedersen, O. Hansen, S. Dahl, I. Chorkendorff, *Angew. Chem. Int. Ed.* **2012**, *51*, 9128–9131.

A robust general concept for monolithic photoelectrochemical cells is reported, which is employed to efficiently split water under solar irradiation without the application of an external bias. It allows to prepare complete water splitting cells by simple means at a low cost. This design should lead to considerable improvements in the field of solar fuels.

artificial photosynthesis, water splitting, silicon, nickel

S. Kasemthaveechok, K. Oh, B. Fabre, J.-F. Bergamini, C. Mériadec, S. Ababou-Girard, G. Loget*

A general concept for solar water-splitting monolithic photoelectrochemical cells based on earth-abundant materials and a low-cost photovoltaic panel

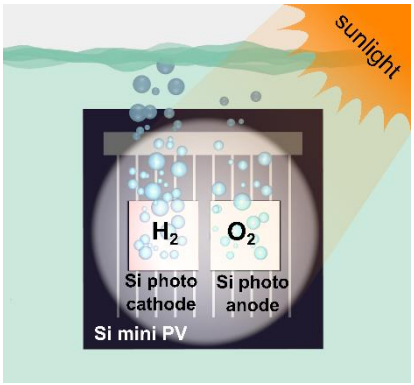

Supporting Information

A general concept for solar water-splitting monolithic photoelectrochemical cells based on earth-abundant materials and a low-cost photovoltaic panel

*Sitthichok Kasemthaveechok, Kiseok Oh, Bruno Fabre, Jean-François Bergamini, Cristelle Mériadec, Soraya Ababou-Girard and Gabriel Loget**

1. Experimental Methods

Reagents. Acetone (MOS electronic grade, Erbatron from Carlo Erba) and anhydrous ethanol (RSE electronic grade, Erbatron from Carlo Erba) were used without further purification. The ultrapure water had a resistivity of 18.2 MΩ cm (Purelab Classic UV). Sulfuric acid (96%, VLSI grade Selectipur) and hydrogen peroxide (30%, VLSI, Sigma-Aldrich) were purchased from BASF and Sigma Aldrich, respectively. NaOH (>98%, ACS reagent) was purchased from Sigma-Aldrich. Boric acid (>99.8%) and $NiCl_2$, $6H_2O$ (99.3%) were purchased from Alfa Aesar. The K-borate buffer was prepared by adding KOH (Sigma Aldrich, >85%) into a 2 M solution of boric acid until the pH reached a value of 9.6.

Surface Preparation. All Teflon vials and tweezers used for cleaning of silicon were previously decontaminated in 3/1 v/v concentrated H_2SO_4/30% H_2O_2 at 105 °C for 30 min, followed by copious rinsing with ultrapure water. *Caution: the concentrated aqueous H_2SO_4/H_2O_2 (piranha) solution is very dangerous, particularly in contact with organic materials, and should be handled extremely carefully.* The *n*- and *p*-type (1-5 Ω cm resistivity, phosphorus- or boron-doped, double side polished, 275-325 μm) (100) silicon wafers and the n^+- and p^+-type (0.001 Ω cm resistivity, phosphorus- or boron-doped, single side polished, 275-325 μm) (100) silicon wafers were purchased from Sil'tronix. All the Si surfaces were degreased by sonication in acetone, ethanol, and ultrapure water for 10 min respectively. The surfaces of the wafers were cleaned in piranha solution at 105 °C for 30 min, followed by rinsing with copious amounts of ultrapure water. The FTO slides (Sigma Aldrich) were cleaned with a detergent (110551, Ecolab) followed by sonication with acetone and ethanol and dried under a Ar flow.

Electrodeposition of Ni NPs. Before the electrodeposition of Ni on the *n*-Si surface (2 x 1 cm^2), an ohmic contact was prepared as follows: *i*) the oxide layer of clean Si wafer was removed by dipping in a diluted HF solution (5/1 v/v ultrapure water/50% aq. HF) for 2 min. Then, the hydrogenated Si (Si-H) surface was quickly dried by an Ar flow, *ii*) InGa eutectic

(99.99%, Alfa Aesar) was applied on the top part of the wafer after scratching with a glass cutter, *iii*) a thin layer of Ag paste (Electron Microscopy Sciences) was painted on the InGa uniformly for covering the InGa contact. After Ag paste dried, the uncoated Si surface was dipped for 2 min in a diluted HF solution (5/1 v/v ultrapure water/50% aq. HF) and quickly dried under an Ar flow. The backside surface was then quickly covered with a hydrophobic adhesive tape (5490, 3M) to prevent electrodeposition on this side. The bare Si-H surface was immersed in the freshly prepared air-equilibrated plating solution that consisted of 20 mM $NiCl_2$,$6H_2O$ and 0.1 M boric acid. The potentiostat used for electrodeposition was a SP 150 (Biologic). The electrodeposition potential was -1.5 V *vs* SCE (SCE, KCl sat.) that was applied for 5 s. After electrodeposition, the coated surface was rinsed with ultrapure water several times and dried with Ar.

Deposition of the Ti and Ni layers. The oxide layer of clean oxidized *p*-Si surface was removed by dipping in a diluted HF solution (5/1 v/v ultrapure water/50% aq. HF) for 2 min, then it was inserted in the chamber of a Leica EM ACE600 coating system fitted with two sputter heads under Ar atmosphere. The 5 nm-thick Ti layer (target purity: 99.8%, Leica) was deposited with a pressure of 1×10^{-2} mbar and a current of 100 mA and the 1 nm-thick Ni layer (target purity: 99.8%, Leica) was deposited with a pressure of 2×10^{-2} mbar and a current of 100 mA.

Electrode fabrication. First, an ohmic contact was performed on the backside of Si wafer by scratching the surface with a diamond glass cutter; then InGa eutectic was applied on the scratched part and the extremity of an electric wire (where the sheath was removed) was deposited on the scratched part. A thin silver paste layer was painted to cover the InGa eutectic contact as well as a part of the wire. After drying of the paste, epoxy resin (Loctite 9460, Henkel) was deposited to shield the backside and frontside of the surface except an active area of 0.45 cm^2 (the confidence interval is ±0.04 cm^2, as based on the standard deviation obtained with 15 electrodes prepared in the frame of this study, the exact

geometrical value was measured using the ImageJ software). The electrode was baked in the oven at 90 ^{o}C overnight to cure the resin, a picture of two electrodes is shown in Figure S8a.

Photoelectrochemical experiments. Three electrode measurements were performed in a three-neck cell comprising a quartz window and gas inlets. The reference was a Hg/HgO (1 M NaOH) electrode and the counter electrode was a Pt cylinder for the CVs shown in Figure 1a or a carbon rod, for the CVs shown in Figure 1b. The cell was filled with 1 M NaOH (measured pH=13.6) that was constantly stirred and Ar gas (Alphagaz, Air Liquide) was degassed for at least 20 min before the experiments. All three-electrode electrochemical experiments were performed under stirring and in Ar saturated conditions. The Si surfaces, prepared as previously described, were used as working photoelectrodes. The light was provided by a solar simulator (LS0106, LOT Quantum Design) equipped with an AM 1.5G filter. The power density of the light source was measured prior to experiments at the position of the photoelectrode using an ILT1400 radiometer (International Light Technologies) to ensure the right value (100 mW/cm^2). Electrochemical measurements were performed with a Zennium potentiostat (Zahner). The potentials versus Hg/HgO were converted into potentials versus reversible hydrogen electrode (RHE) using the following relation (the measured pH of the NaOH solution was 13.6):

$$E_{RHE} = E_{Hg/HgO} + 0.098 + 0.059pH = E_{Hg/HgO} + 0.9004$$

The activation of the *n*-Si/Ni NPs$_{act}$ photoanode was performed by applying 100 CV cycles from -0.7 V to +2 V vs Hg/HgO at 100 mV s^{-1} under simulated sunlight. The two electrode-measurements were performed in the electrolysis cell shown in the photograph of Figure S9a with shorted counter and reference electrodes, and with spot light of the solar simulator covering both photoelectrodes. All reported potentials were intentionally not corrected by the ohmic drop. The CVs reported in this work were recorded at 100 mV s^{-1} except for the FTO / Ni film anode (green CV in Figure 1a) that was recorded at 20 mV s^{-1} in order to prevent the Ni^{3+}/Ni^{2+} redox wave to hide the OER onset.

PEC preparation. The PV panel (Cebekit C-0138) was purchased from the website Eclats Antivols. First, the backside of the PV panel was coated with epoxy resin and the photoelectrodes were immobilized in the middle of the frontside of the PV panel using the same resin (Loctite 9460, Henkel). The assembly was cured overnight at 40 °C. A picture of the PEC is shown in Figure S8b.

PEC measurements. The PEC assembly was placed in the home-made glass, cell shown in Figure S9a, and the electrolyte was poured into the cell to immerse the entire PEC. The cell was placed at the appropriate distance of the solar simulator (Figure S8c) and the height of the cell was adjusted in order to locate the illumination spot in the middle of the PV panel. The photoanode and the photocathode wires were respectively connected to the positive and the negative wires of the PV panel by short wires and crocodile clips or by welding. Eventually, the Zennium potentiostat was connected in series between a photoelectrode and the PV panel in a two-electrode fashion (with shorted counter and reference electrodes). In this case, CAs were recorded with no applied potential (E = 0 V) to measure the current flowing through the system under illumination. No diaphragm was used, except for the experiments shown in Figure 2b.

Illumination-controlled experiments. In order to precisely control the size of the spot illuminating the PEC, a diaphragm was adapted on the cell, as shown in Figure S9b,c. As the beam is uniform to ±10% over 4.9 cm^2 (100 mW cm^{-2}), the aperture area was chosen smaller than this value to ensure a precise measurement. The aperture area was measured before each experiment which allowed determining the value of P_{in}. For measurements performed without a diaphragm, analysis of the spot intensity allowed to estimate a value of P_{in} of 820 mW. The electrolysis current was recorded for 15 min for several aperture diameters (Figure S10).

Gas detection. The PEC wires were welded and the cell was sealed using the top part shown in the right part of Figure S9a. The electrolyte was 1M NaOH, previously degassed with Ar. The electric wires that were integrated in the top part of the cell allowed to measure the

current passing through the PEC and the CA measurements were performed as described previously for PEC measurements. The resulting CA curves (Figure S11) were integrated to measure the charge delivered during electrolysis. H_2 was detected using aClarus 580 (Perkin Elmer) GC system equipped with a thermal conductivity detector. H_2 production was quantitatively detected using Shincarbon (2 m in length and 1 mm internal diameter) and Haysep (2 m in length and 1 mm internal diameter) columns. The temperature was held at 100 °C for the detector and 40 °C for the oven. The carrier gas was argon flowing at 8 mL/min at constant pressure. The injection was performed via a 100 μL gas-tight syringe (Hamilton). Calibration curves for H_2 were determined separately by injecting known quantities of pure gas. The amount of O_2 ($\%_{O_2}$) in the headspace was detected using a Neofox detection system (Ocean Optics) and a patch (FOSPOR) that was placed inside in the top part of the cell. A two point calibration curve was recorded before the measurements. The number of moles of gases, ($n_{H_2\,exp}$, $n_{O_2\,exp}$), was calculated as follow:

$$n_{gas\,exp} = \frac{PV_{hs}}{RT} \times \%_{gas_{det}}$$

Here R is the ideal gas constant, T = 298.15 K, P is the atmospheric pressure, V_{hs} is the headspace volume in the cell, $\%_{gas_{det}}$ is the concentration of gas detected in the system (either H_2 or O_2). The concentration of gas inside the solution phase can be calculated using Henry's law, however, the corresponding number of moles was so small, (more than two orders of magnitude smaller than the quantity of gas in the headspace), that we have not taken it into account in our results.

Surface characterization. Scanning electron microscopy (SEM) was performed using a JSM 7100F (JEOL). SEM picture analysis was performed using the ImageJ software. AFM images were acquired on a NT-MDT NTegra microscope in semi-contact mode with FM tips (resonance frequency around 60 kHz). The images were treated and analyzed with the open-source Gwyddion software. The value of NPs diameters were extracted from ImageJ analysis.

XPS measurements were performed with an Al source ($h\nu$ = 1486.6 eV) using a VSW HA100 photoelectron spectrometer with a hemispherical photoelectron analyzer, working at an energy pass of 20 eV for survey and resolved spectra. The experimental resolution was 1.0 eV. C1s set at 284.8 eV is used as the energy reference for all the analyses.

2. Supplementary figures

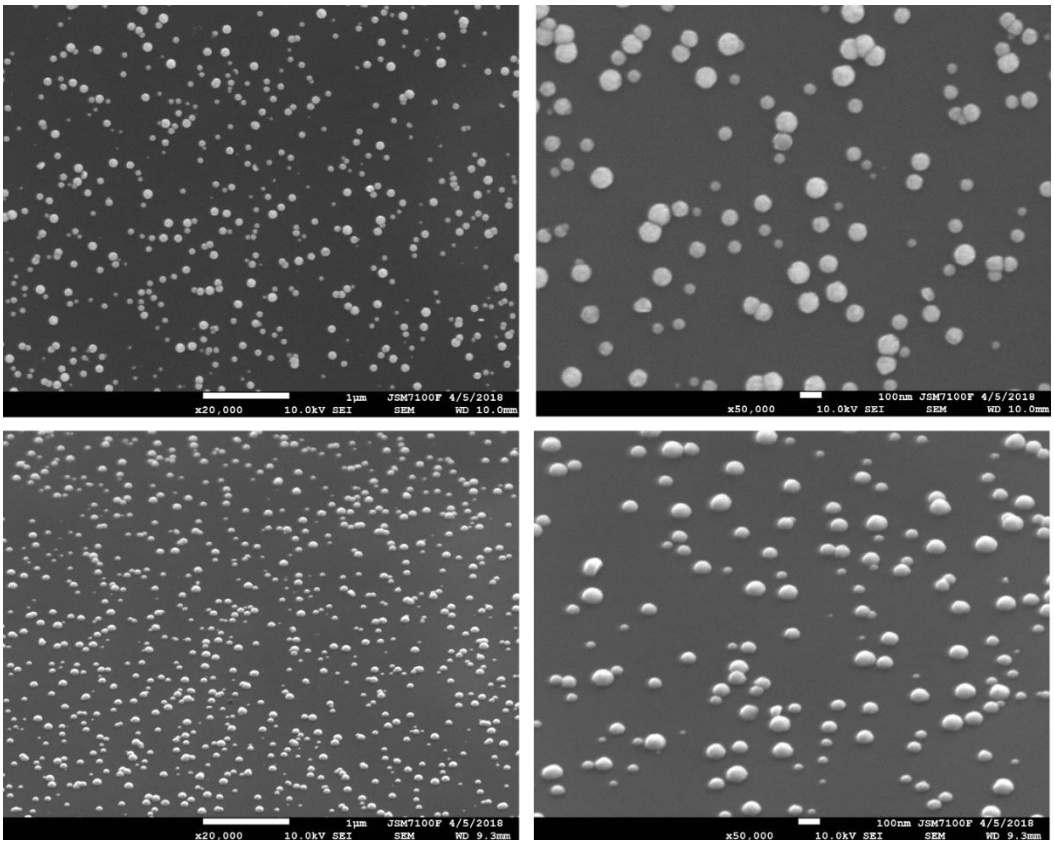

Figure S1. SEM images showing Ni NPs electrodeposited on *n*-Si. Top row: top views. Bottom row: tilted views. The scalebars equal to 1 µm in the left column and 100 nm in the right column.

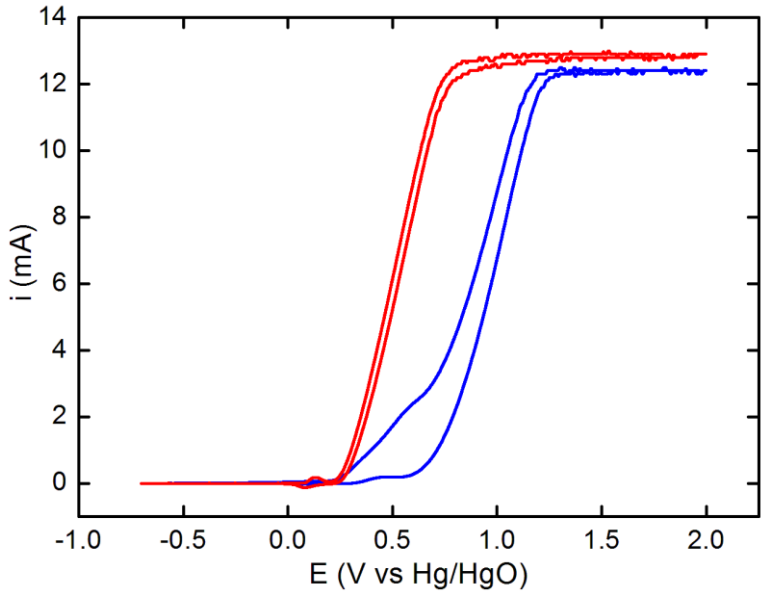

Figure S2. CVs obtained before (blue) and after (red) the photoelectrochemical activation of a Ni/*n*-Si photoanode. The photoelectrochemical activation consisted in applying 100 CV scans between -0.7 to +2 V under AM 1.5G illumination in O_2-saturated 1 M NaOH under stirring at 100 mV s^{-1}.

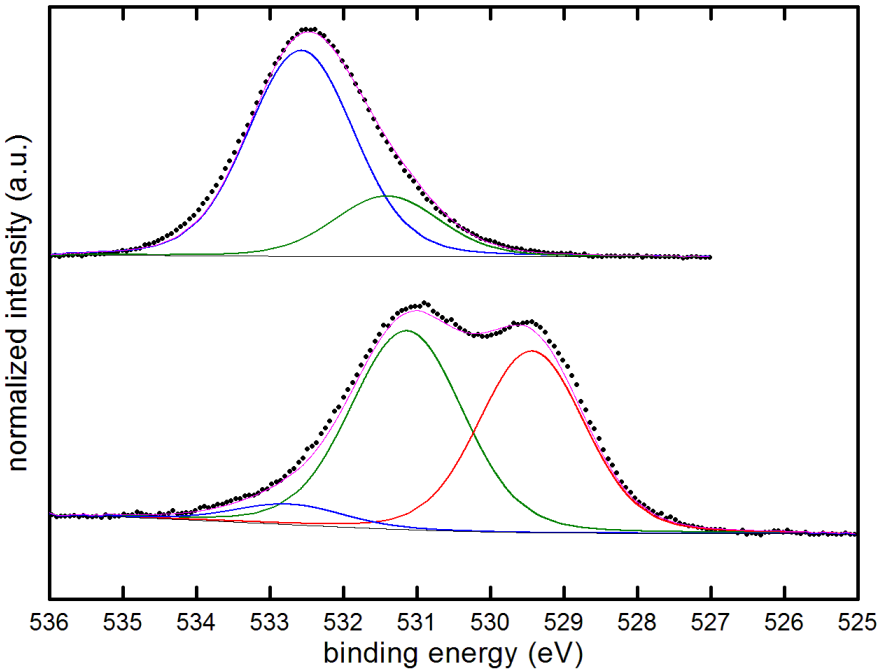

Figure S3. XPS spectra showing the O 1s region, measured for the *n*-Si/Ni NPs_{act} photoanode (top) and the *p*-Si/Ti/Ni photocathode (bottom). Black disks are experimental data, grey thin lines are Shirley backgrounds. Thick colored lines are fits corresponding to SiO_x (blue), Ni oxides ($Ni(OH)_2$, NiO or NiOOH, (green)) and TiO_2 (red); the pink thin line is the fit envelope.

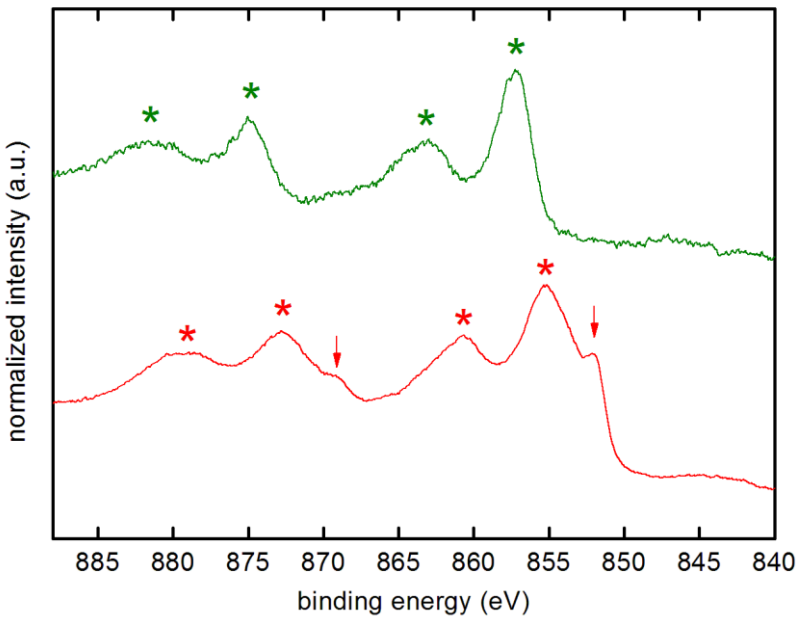

Figure S4. XPS spectra showing the Ni 2p region, measured for the *n*-Si/Ni NPs_{act} photoanode (green line) and the *p*-Si/Ti/Ni photocathode (red line). Arrows indicate Ni^0 peaks and asterisks indicate Ni oxides or hydroxides peaks.

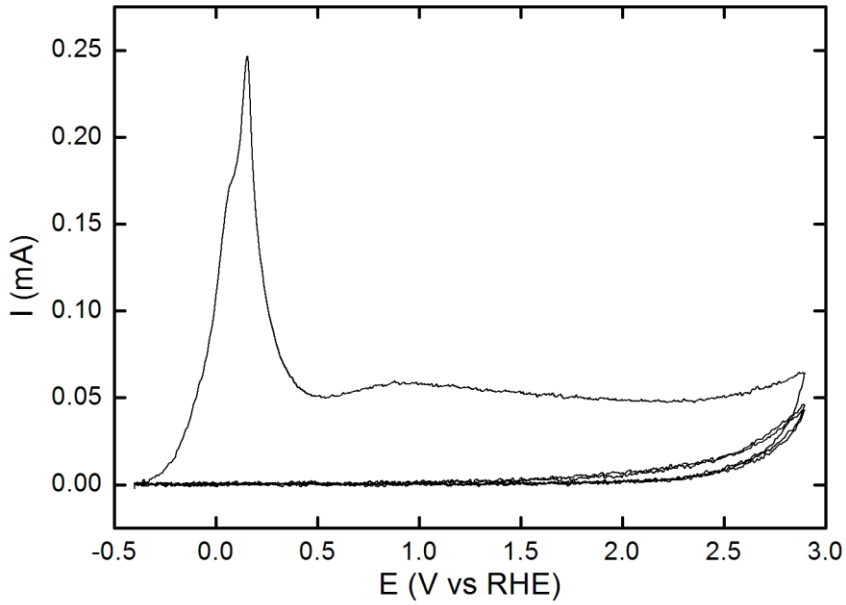

Figure S5. Three successive voltammetric cycles recorded in Ar-saturated 1 M NaOH under AM 1.5G illumination at 100 mV s^{-1} with a *n*-Si photoanode. ***The presence of a passivation peak at +0.15 V at the first cycle and the considerable current decay at the subsequent cycles clearly indicates the anodic passivation of the Si surface with an insulating SiO_x layer.***[1,2]

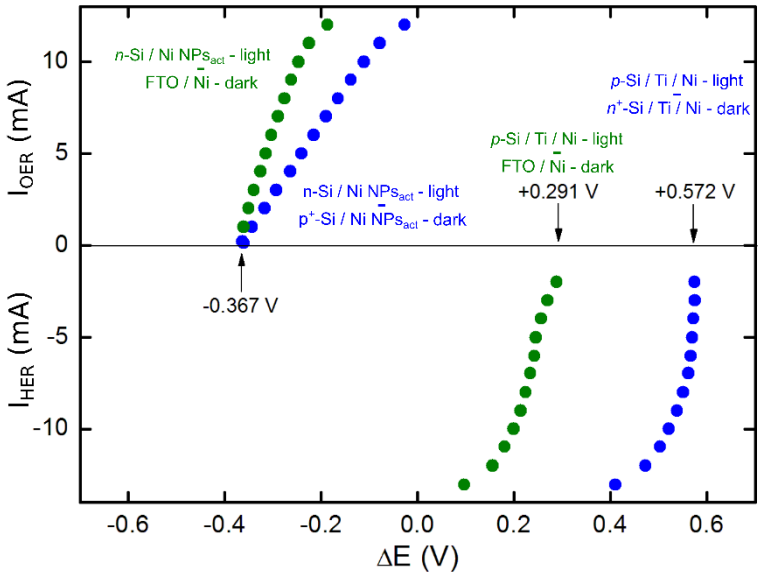

Figure S6. Plots showing the differences of OER and HER potentials between the photoactive electrodes under illumination and the non-photoactive electrodes in the dark as a function of current for the anodes (left) and for the cathodes (right).

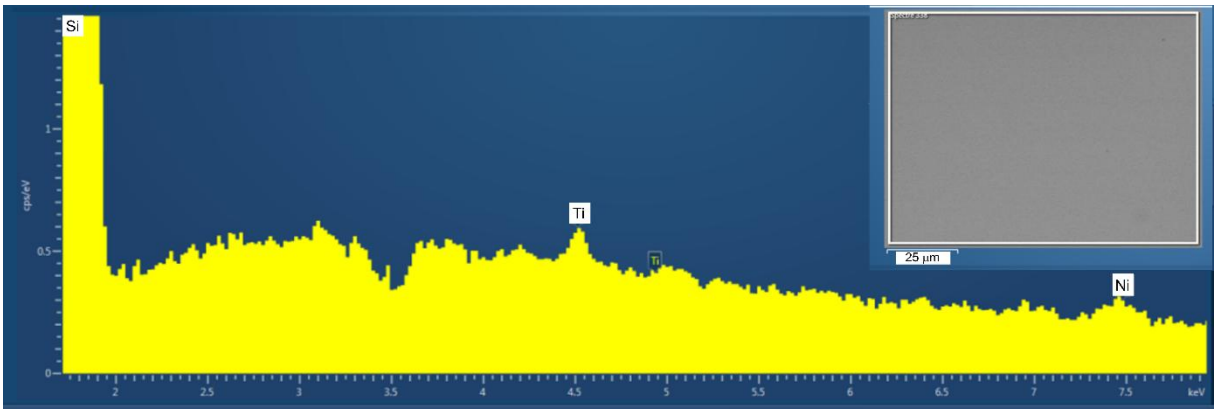

Figure S7. EDS spectrum recorded on the region shown in the inset for the *p*-Si/Ti/Ni photocathode.

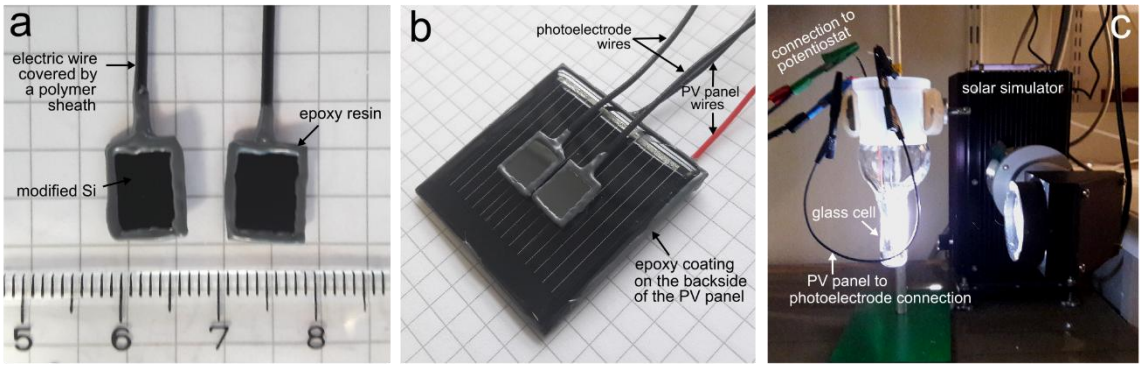

Figure S8. a) Photographs of two Si photoelectrodes. b) Photograph showing the PEC where the two Si photoelectrodes are immobilized on a PV panel. c) Photograph showing the PEC in the cell filled with the electrolyte and illuminated with a solar simulator.

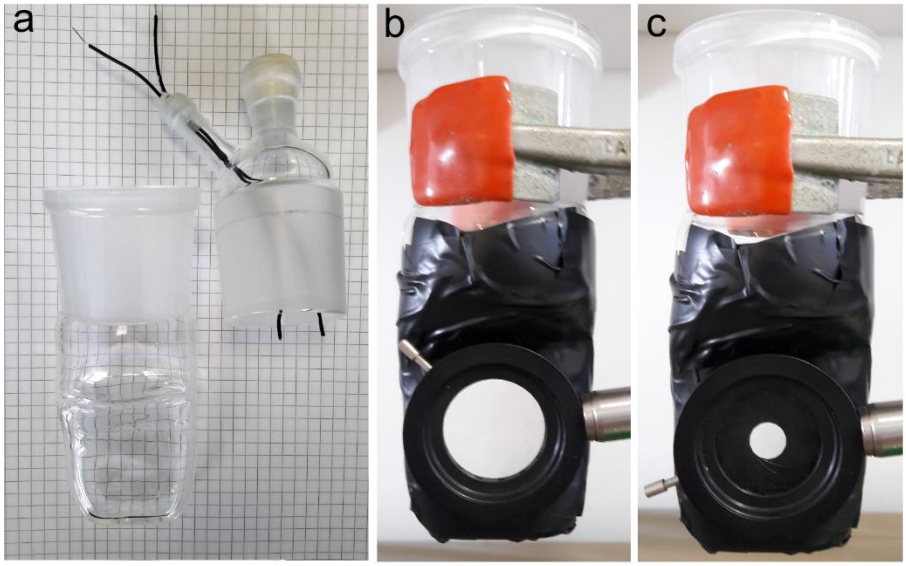

Figure S9. a) Photograph showing, on the left, the glass cell used for the water-splitting experiments with the PEC, the right element is the top part that was used in sealed conditions, such as the gas detection experiments of Figure 2e (note that the two wires allow a connection of the PEC with the potentiostat to record *in-situ* the current flowing through the PEC). b) Photograph showing a diaphragm adapted on the glass cell in a fully opened position. c) Photograph showing the diaphragm in a partially opened position.

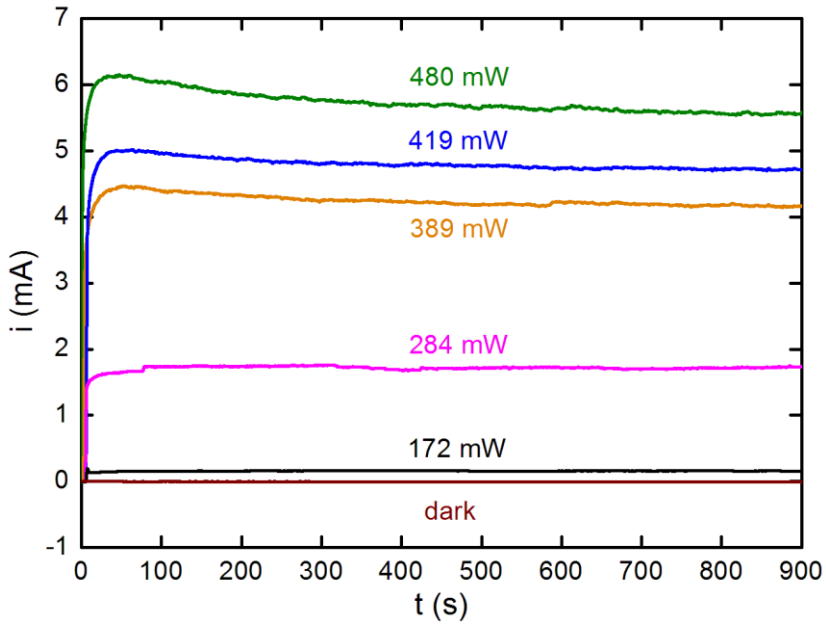

Figure S10. CA curves showing the current flowing through the PEC under illumination with different beam diameters of AM 1.5G light.

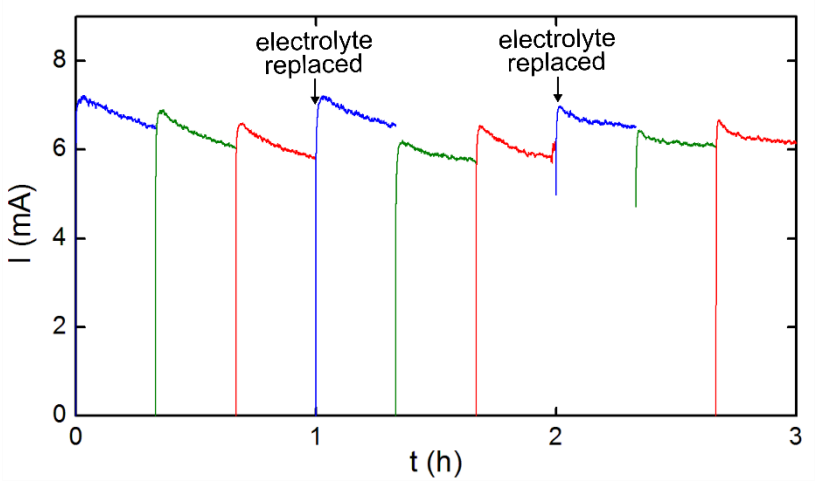

Figure S11. Curves showing the variation of the current flowing through the illuminated PEC during the preparative-scale water-splitting experiments in 1 M NaOH.

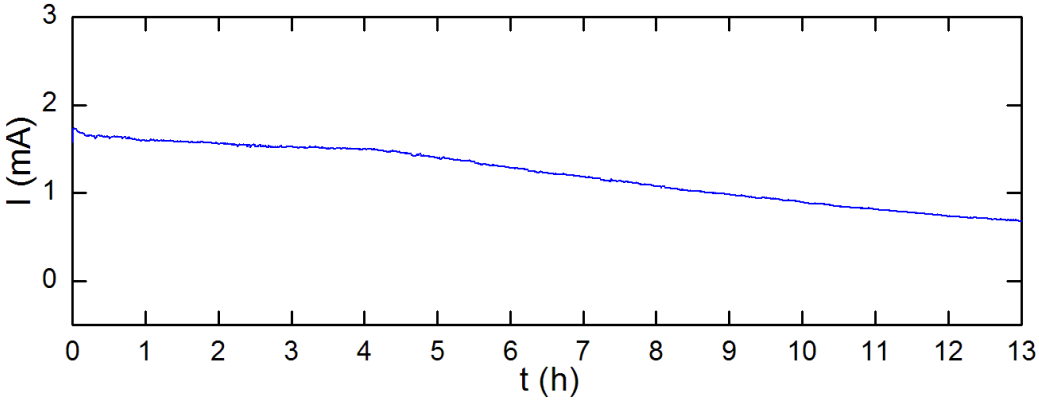

Figure S12. Current flowing through the illuminated PEC during preparative-scale water-splitting experiments in 2 M K-borate buffer (pH = 9.6).

3. Supplementary tables

Table S1. Values of the light spot area A_{ill}, the corresponding illumination power P_{in}, the current I determined by CA, and the corresponding solar-to-H_2 efficiencies η_{STH}.

	A_{ill} (cm²)	P_{in} (mW)	I (mA)	η_{STH} (%)
1 M NaOH	no diaphragm	820	5.95	0.89
	4.80	480	5.73	1.47
	4.19	419	4.80	1.41
	3.89	389	4.25	1.34
	2.84	284	1.72	0.74
	1.72	172	0.16	0.11
K-borate buffer	no diaphragm	820	1.68	0.25

4. References

1 P. Allongue, V. Costa-Kieling and H. Gerischer, *J. Electrochem. Soc.* , 1993, **140**, 1018–1026.

2 J. W. Faust and E. D. Palik, *J. Electrochem. Soc.* , 1983, **130**, 1413–1420.